ACS Sustainable Chemistry & Engineering

pubs.acs.org/journal/ascecg

Research Article

5−5 Lignin Linkage Cleavage over Ru: A Density Functional Theory Study

Qiang Li and Dionisios G. Vlachos*

Cite This: *ACS Sustainable Chem. Eng.* 2021, 9, 16143−16152

Read Online

ACCESS | Metrics & More | Article Recommendations | Supporting Information

ABSTRACT: Lignin is the most abundant natural, aromatic-containing biopolymer. Among all the C−C and C−O bonds being cleaved in catalytic fractionation, the 5−5 linkage is the strongest, and its scission requires harsh conditions. Theoretical investigations of the mechanism and kinetics could provide insights into developing better catalysts but are essentially lacking. We perform extensive density functional theory calculations on 2-methoxy-1,1′-biphenyl, a model compound, with various substitutions at all ring locations on Ru(0001). We analyze the competition between the 5−5 bond cleavage and the defunctionalization of the side functional groups at multiple degrees of depolymerization. The role of ring functional groups in the adsorption of lignin oligomers and the 5−5 bond scission and, conversely, the effect of the aromatic group on the $-OCH_3$ decomposition are also discussed. We show that increasing the number of methoxy groups decreases the C−C barrier, and thus, we expect the following depolymerization ranking: grass > softwood > hardwood. While Ru exposes modest 5−5 bond scission reaction barriers from some intermediates, rapid side group chemistry prevents the formation of these intermediates; instead, scission happens most probably from defunctionalized compounds whose C−C scission barriers are high. Our results also expose the existence of multiple Brønsted−Evans−Polanyi relations in the catalytic transformation of biphenyl-based molecules that open up the possibility of modeling depolymerization of large lignin chains.

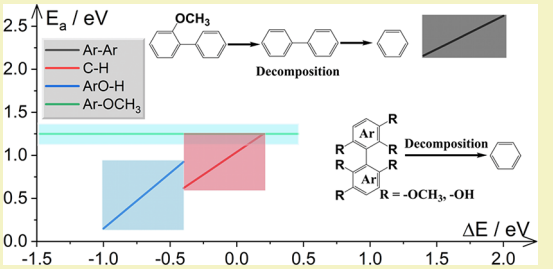

KEYWORDS: *lignin, depolymerization, heterogeneous catalysis, scaling relationships, substitution effects*

INTRODUCTION

Lignin is a cross-linked phenolic biopolymer and the largest natural source of aromatic compounds on Earth.[1] The diversity of lignin stems from the different ratios of three monolignols (Figure 1, p-coumaryl (H), coniferyl (G), and sinapyl alcohols (S)) and the C−C and C−O linkages holding the polymer together. Lignin can provide aromatic platform compounds, such as BTX (benzene, toluene, and xylene), phenols, and bio-oil, via pyrolysis and oxidative and reductive depolymerization.[2,3] The bio-oil needs to be catalytically upgraded, for example, by hydrodeoxygenation, to produce ready-to-use fuels and chemicals.[4]

During the lignin depolymerization, C−C and C−O bonds dissociate. The 5−5 linkage between aromatic groups accounts for 10−25% of all bonds and up to 40−50% of all C−C bonds.[3] Due to its strength, high temperatures and active catalysts are required to achieve decent monoaromatic yield. Among metal catalysts, Ru, Pd, Pt, Ni, and Rh have been exploited.[5,6] Ru is, in general, effective for the catalytic transformation of biomass-derived compounds in the aqueous phase.[7−9] Ru is selective for C−O bond hydrogenolysis,[10] C−C bond scission, and hydrogenation. Recently, Wang et al.[3] used $Ru/NbOPO_4$ to cleave C−C and C−O bonds in one-pot lignin and reported a higher lignin monomer yield using the nitrobenzene oxidation method. They also investigated C−C bond breaking from half-hydrogenated biphenyl (phenyl cyclohexane) over metal oxides (Nb_2O_5, TiO_2, ZrO_2, and γ-Al_2O_3)[11] and elucidated the superior catalytic performance of Nb_2O_5 on C−C cleavage via its strong binding toward the adsorbates and high activity toward protonation.

Compared to many experimental studies on lignin depolymerization, modeling has been less common and focused on adsorption,[12,13] the β-O-4 linkage cleavage mechanism,[14−16] and hydrodeoxygenation of phenolic compounds.[17−21] Mechanism studies on C−C bond cleavage over metal catalysts are much less conducted. Due to the large fraction of C−C units in lignin, theoretical investigations are urgently needed to understand the mechanism and provide guidance for catalyst development.

Biphenyl is an excellent model compound for studying the 5−5 bond cleavage but is a little too simplistic given the diversity of lignin sources and functional diversity at C1, C3, and C4 positions (Figure 1). These functional groups affect the

Received: July 17, 2021
Revised: November 8, 2021
Published: November 19, 2021

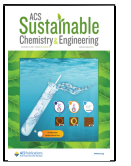

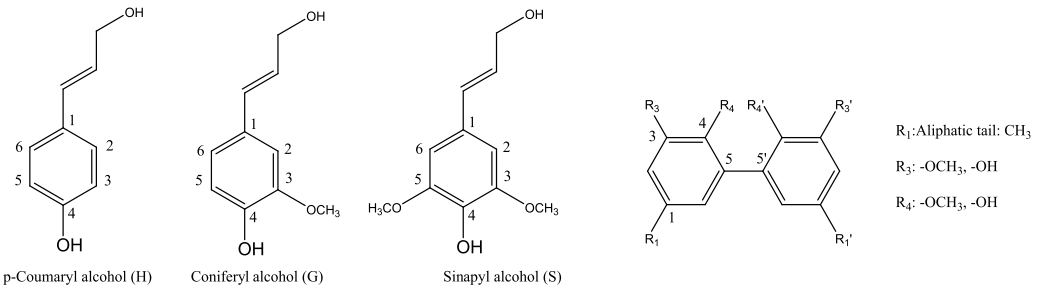

Figure 1. Structures of monolignols and possible substitution groups on the 5−5 linkage model (biphenyl).

5−5 bond energies and the steric and electronic interactions of the aromatic units with the catalyst. C−H and C−O bond scissions in the functional groups (e.g., aliphatic tails, such as $-OCH_3$) are also absent in the biphenyl.

The complex and large model-lignin compounds limit the density functional theory (DFT) calculations for heterogenous catalysis due to the large atom numbers and the unit cell size in the system. This challenge can be circumvented using scaling relations. Specifically, scaling relations between thermodynamic and kinetics, such as Brønsted−Evans−Polanyi (BEP) relations and initial state or final state scalings (ISS or FSS), can predict reaction barriers. The relations exist for small molecules[22−24] and biomass-derived compounds, e.g., methanol,[25] ethanol,[26] ethylene glycol,[27] and furan derivatives.[28] Reported linear scaling relationships for binding energies also exist for small intermediates like CH_x, OH, OOH, and SH_x.[29−31] However, scaling relations of bond dissociations in large molecules, such as lignin model compounds, are rarely reported. For lignin compounds, C−H, C−O, C−C, and O−H bond scissions can occur at the prime chains, such as β-O-4, 4-O-5, and the functional groups, e.g., $-OCH_3$, attached to the aromatic rings. The geometries of lignin compounds are primarily dictated by the aromatic units, and substitutions can disturb the π−d orbital interactions and affect the bond dissociation to a different degree. Conversely, the interactions of the functional groups with the catalyst surface are either hindered or promoted by the aromatic units. This complexity calls for calculations on biphenyl-like molecules and substitutional effects on the ring.

Here, we perform DFT calculations on the 5−5 linkage bond dissociation of biphenyl and its substituted structures on Ru(0001). We analyze the substitution effects on the adsorption energies, activation barriers, and reaction energies. We draw a BEP relation between the adsorption energies and reaction barriers. Dispersion effects are also discussed. The reaction network of 5−5 linkage transformation is showcased for the 2-methoxy-1,1′-biphenyl model compound, but the results can be applied to many other lignin-derived compounds. The effects of $-OCH_3$ decomposition on 5−5 bond breakings and of the aromatic units on the $-OCH_3$ decomposition are also discussed.

THEORETICAL METHODS

DFT calculations were performed using the Vienna *ab initio* Simulation Package (VASP).[32−34] The exchange-correlation energies were obtained via the generalized gradient approximation (GGA) with the Perdew−Burke−Ernzerhof functional (GGA-PBE).[35] Valence states were expanded in plane waves with a cutoff energy of 450 eV. The inner electrons were modeled with a projector augmented wave (PAW) pseudopotential.[36,37] Van der Waals interactions were considered via Grimme's DFT-D3 method.[38] Gas-phase molecules were relaxed in a box of 20 × 20 × 20 Å^3. The optimized lattice parameters of Ru using DFT and DFT-D3 methods are 2.714 Å (c/a = 1.579) and 2.690 Å (c/a = 1.582), respectively, close to the experimental values of 2.706 Å (c/a = 1.582).[39] These lattice parameters were applied to build the slab models. A p-(6 × 6)-Ru(0001) slab with four layers was adopted as the catalyst model. The two uppermost layers were allowed to relax, while the rest were frozen to their bulk positions. Gamma-centered k-point meshes were generated through the Monkhorst−Pack method with 3 × 3 × 1 and 2 × 2 × 1 sampling for p-(4 × 4) and p-(6 × 6) slabs, respectively. The climbing image nudged elastic band (CI-NEB) approach[40,41] and the quasi-Newton algorithm were employed to locate transition states (TSs).

RESULTS AND DISCUSSION

Adsorption and Dissociation of Biphenyl and the Effect of Dispersion Corrections. The effect of dispersion corrections was investigated by comparing the results with and without D3 corrections with benzene as the probe molecule. As shown in Figure 2, three surface sites (bridge, fcc, and hcp) with two orientations (0° and 30°) for each were considered. For instance, the hcp-30° is obtained by rotating the hcp-0° structure by 30° along the vertical axis across the ring center.

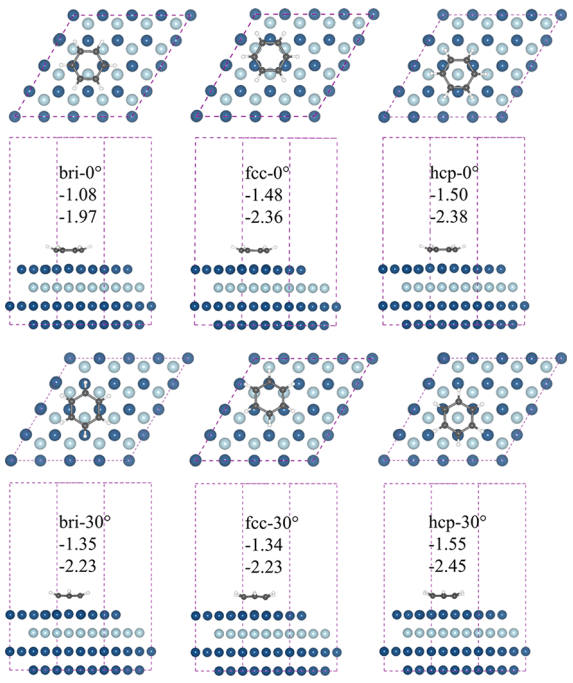

Figure 2. Top and side views of different benzene adsorption orientations on Ru(0001). The upper and lower values correspond to the adsorption energies from DFT and DFT-D3 calculations, respectively.

https://doi.org/10.1021/acssuschemeng.1c04838
ACS Sustainable Chem. Eng. 2021, 9, 16143−16152

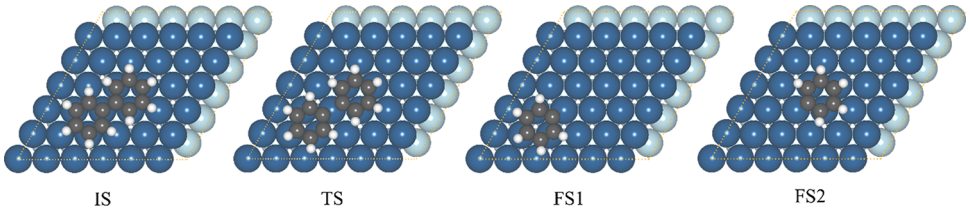

Figure 3. Most stable adsorption geometry of biphenyl on Ru(0001) and the corresponding transition state (TS) and final states (FSs) upon the 5−5 bond cleavage.

The most stable adsorption site without dispersion is the hcp-30° with a binding energy of −1.55 eV. Three C atoms (labeled as C^{top}) are atop Ru atoms and the rest above fcc sites (C^{fcc}), in agreement with low-energy electron diffraction structures of C_6D_6 on Ru(0001).[42,43] The average Ru−C distance (d(Ru-C)) in the hcp-30° structure is 2.15 Å, and the C^{top} atoms are further apart from the surface in the z-direction than the C^{fcc} atoms by 0.07 Å (Δz^C), close to the experimental values of 2.11 (d(Ru−C)) and 0.08 Å (Δz^C), respectively.[42] Dispersion corrections do not change the order of binding energies on different sites, but the adsorption energies increase significantly, on average by 0.90 eV. The most stable D3-corrected geometry (hcp-30°) is slightly different with d(Ru−C) and Δz^C are elongated by 0.002 and 0.01 Å, respectively. The results imply that D3 corrections enhance binding energies but slightly affect adsorption geometries and their relative energies.

Figure 3 illustrates the most stable initial state (IS), transition state (TS), and final state (FS) in the 5−5 bond scission in biphenyl. The IS structure has the aromatic rings above the hcp sites with an orientation angle of 30°, similar to the most stable benzene adsorption structure. The adsorption energy without dispersion is −2.49 eV. The 5−5 bond length in the IS is 1.466 Å and is elongated by 50% to 2.199 Å in the TS. In FS1 and FS2, the unsaturated C atoms (C^5) are above the hcp and fcc sites, respectively, and FS1 is more stable than FS2 by 0.12 eV. The 5−5 bond scission is an endothermic reaction with a reaction barrier and energy of 2.15 and 1.17 eV, respectively. When dispersion corrections are included, the binding energy of the IS is increased by 0.85 eV per aromatic unit and reaches −4.19 eV for biphenyl. Again, no significant geometric changes are observed from dispersion corrections. The 5−5 bond lengths in the IS (1.466 Å) and the TS (2.200 Å) are almost identical to the nondispersion results. Minor effects of D3 corrections on the C−C distances in the IS and TS suggest that the reaction barrier (2.20 eV) and energy (1.15 eV) are practically unaffected.

Reaction Network and Energetics in the Deconstruction of 2-Methoxy-1,1′-biphenyl. 2-Methoxy-1,1′-biphenyl (structure A0 in Figure 4) is used as a model compound. The methoxy group connected to the ring in A0 mimics the α-O-4 or β-O-4 linkages. Aryl (Ar)−Ar, Ar−O, O−CH_3, C−H, Ar−H, and O−H bond scissions are also included in the reaction network. The aromatic ring hydrogenations and decompositions of the nonring species are left out to reduce the size of the network. Specifically, Ar−Ar (5−5 bond) cleavage proceeds in the horizontal direction to form structures B, followed by hydrogenations of the unsaturated carbon of the rings to structures C. In the vertical direction, the reactions mainly act on the −OCH_x functional group and are analogous to those in the CH_3OH decomposition[25] (where Ar, the aryl unit, replaces a single H atom): they include the bond scissions of C−H, Ar−OCH_3, O−CH_3, O−H, and Ar−H.

The reaction barriers E_a and energies ΔE from DFT-D3 calculations are tabulated in Table S1. In Figure 4a, the reported energies are labeled as $E_a/\Delta E$. The species converted directly to A4 and A6 are also marked before the energies shown next to A4 and A6, e.g., A0: 1.10/−1.50 eV by A4 represents the energies for the reaction A0 → A4. The elementary reaction with the lowest barrier from each species is marked in red. Starting from A0, a C−H bond dissociation (A0 → A1) occurs first on −OCH_3 with a barrier/reaction energy ($E_a/\Delta E$) of 0.70/-0.28 eV, followed by the O−CH_2 bond breaking (A1 → A4) with energies of 0.09/−1.51 eV to produce 2-phenylphenoxy.

In addition, the C−H bond scission A1 → A2 has a low barrier of 0.33 eV. From A2, the ArO−CH bond breaking (A2 → A4) is barrierless. The 5−5 and C−O bonds in A4 are difficult to break; they possess high barriers of2.31 and 2.15 eV, respectively. Thus, hydrogenation to 2-phenylphenol (A5) takes place instead. From A5, the C−OH bond scission barrier is lower than that of 5−5; the reaction is followed by hydrogenation to biphenyl (A6 → A7). The 5−5 bond scission is easier in A7, i.e., upon complete defunctionalization. The energetically preferred reaction path is A0 → A1 → A4 → A5 → A6 → A7. A competitive path from A2, which is the dehydrogenation product of $ArOCH_2$* (A1), exists: A0 → A1 → A2 → A4 → A5 → A6 → A7. In addition, the decomposition can also proceed via a shorter reaction path: A0 → A6 → A7, in which the direct Ar−OCH_3 bond breaking occurs, followed by ring hydrogenation. The bond-breaking barrier of Ar−OCH_3 (0.93 eV, A0 → A6) is 0.10 eV lower than that of the Ar−OH bond scission (1.04 eV, A5 → A6). Based on the above simple energy analysis, the initial C−H and Ar−O bond breakings from Ar−OCH_3, the ArO* hydrogenation, and the Ar−OH bond breakings are crucial in the reaction network and A4 and A6 appear as two key intermediates. The preferred pathway is summarized in Figure 4b.

The reaction energy profile of the preferred elementary steps in the reaction network is shown in Figure 5a,b. The reactions related to the aromatic ring and functional groups tangle with each other. The reaction network is simplified into decomposition and hydrogenation. In the decomposition path, the products are benzene and surface species (C* and O*) and the overall reaction is exothermic by 1.32 eV. C* and O* cover the surface sites, leading to catalyst deactivation. Thus, H_2 is crucial to removing the surface species and freeing up the catalytic sites. The hydrogenation pathway leads to the formation and desorption of H_2O and CH_4. The overall reaction is exothermic by −0.90 eV.

Methoxy is an influential group in lignin as it determines the monolignol type (Figure 1) and its degree of defunctionaliza-

https://doi.org/10.1021/acssuschemeng.1c04838
ACS Sustainable Chem. Eng. 2021, 9, 16143−16152

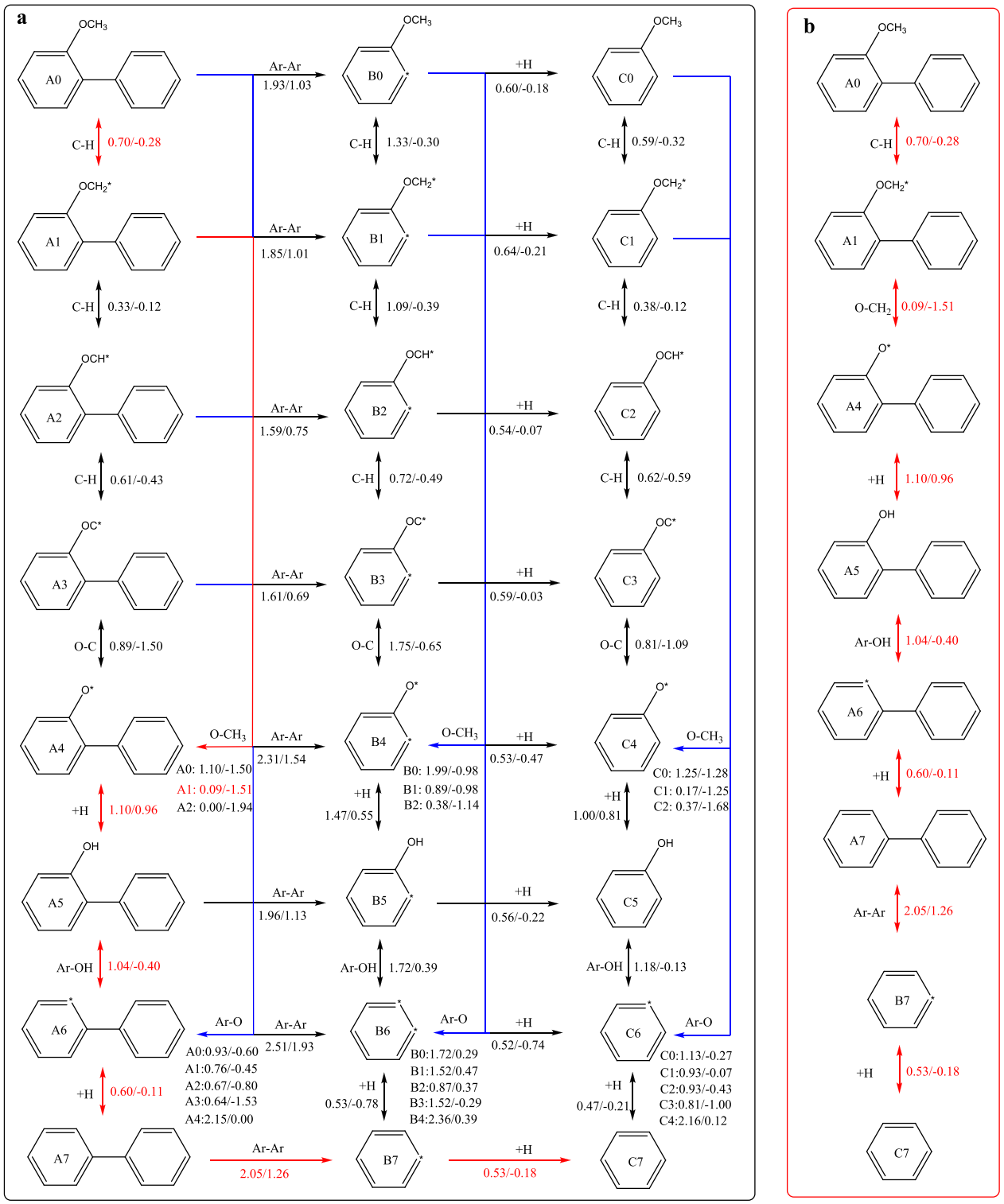

Figure 4. (a) Reaction network of catalytic depolymerization of 2-methoxy-1,1′-biphenyl. The vertical direction shows the decompositions from the $-OCH_3$ group (structures A; left column), and the horizontal direction depicts the 5−5 bond-breaking reactions to structures B (middle column), followed up by hydrogenation to structures C (right column). The arrows indicate the type of bond scission. The numbers indicate the reaction barriers and energies from DFT-D3 calculations ($E_a/\Delta E$, both in eV). The numbers by the $O-CH_x$ and Ar−O arrows at the lower part of the graph refer to oxygen−carbon bond scission of the functional group and complete deoxygenation of the ring, respectively, from the corresponding A_n structure. (b) Preferred paths toward methoxy decomposition and 5−5 bond scission as indicated by the red arrows in panel (a).

tion affects the 5−5 scission barrier. As shown in Figure 5c, the 5−5 scission barriers in A2 and A3 are much lower (1.59 and 1.60 eV, respectively) than in the other intermediates of path A. For example, the 5−5 bond is particularly hard to break in A4 and A6. From the energetic viewpoint, the 5−5 bond breaking in A2 or A3 is preferred. However, C−H dehydrogenation of the methoxy group followed by the ArO−C scissions from $ArO-CH_2$* and ArO−CH* possesses

https://doi.org/10.1021/acssuschemeng.1c04838
ACS Sustainable Chem. Eng. 2021, 9, 16143−16152

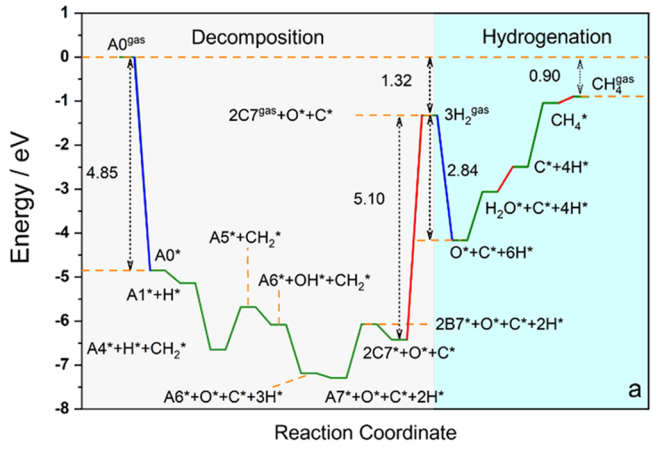

Elementary Steps

Steps	Description	Reactant→Product
1	A0 adsorption	$A0^{gas}$→A0*
2	C—H bond breaking from -OCH_3	A0*→A1*+H*
3	O—CH_2 breaking from -OCH_2	A1*→A4*(phenoxy)+CH_2*
4	O—H bond formation	A4*+H*→A5*(phenol)
5	$C^{aromatic}$—OH bond breaking	A5*→A6*+OH*
6	Small Species decomposition	OH*+CH_2* →O*; H*, C*
7	$C^{aromatic}$—H bond formation	A6*+H*→A7*(biphenyl)
8	5—5 bond breaking	A7*→2B7*(phenyl)
9	Phenyl hydrogenation	B7*+H*→C7*(benzene)
10	Benzene Desorption	C7*→$C7^{gas}$
11	H_2O formation	O*+2H*→H_2O*
12	H_2O desorption	H_2O*→H_2O^{gas}
13	CH_4 formation	C*+4H*→CH_4*
14	CH_4 desorption	CH_4*→CH_4^{gas}

b

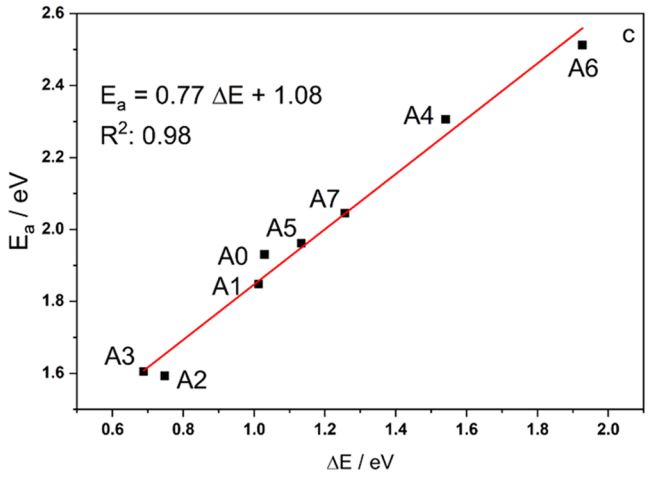

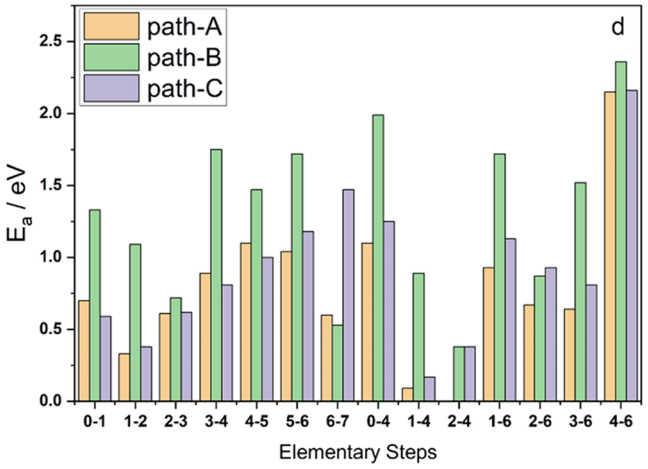

Figure 5. (a) Reaction profile of the most preferred steps in the reaction network by taking gas-phase energies of A0 and H_2 as a reference, (b) description of the reaction steps, (c) BEP relationship for 5−5 barriers *vs* reaction energies on Ru(0001) of species A_n, and (d) reaction barriers of elementary reactions in paths A, B, and C. The reactions are labeled based on the species numbers. For instance, reaction 0-1 in path A stands for C−H bond breaking from species A0 to A1. See Figure 4 for species notation.

much lower barriers. In summary, the 5−5 bond-breaking barriers are much higher than other reactions in all functionalization stages from A0 to A6 and most probably occur after the complete decomposition of the −OCH_3 functional group. It is also clear that mild dehydrogenation followed by demethylation and eventually hydrodeoxygenation, leading to a double aromatic ring, is energetically favorable before Ar−Ar scission can happen. As a result, the lower barrier Ar−Ar bond scissions in A2 and A3 are kinetically irrelevant on Ru. This also explains why so harsh conditions are needed for the 5−5 C−C bond scission. Reducing the lifetime of A4 and A6 species and stabilizing the A2 and A3 species over the catalyst would facilitate the 5−5 bond scission. A good BEP relationship with an R^2 of 0.98 and a mean absolute error of 0.03 eV (Table S3) is found for the 5−5 bond scissions from A0 to A7 that can efficiently predict the reaction barriers of 5−5 bond breakings in other lignin structures. BEPs for Ar−H, Ar−O, Ar−OH, and ArO−H are also good (Table S3).

The side reactions from −OCH_3, such as O−C and C−H bond scissions, are affected by the aromatic groups. The reactions in the vertical direction (Figure 4) are methanol-like decomposition reactions where the aryl groups are replaced by H atoms. The role of the aromatic groups in C−H, C−O, and Ar−O bond scissions in −OCH_3 was investigated using the methanol decomposition network (path D, Figure S1) as a reference. As shown in Figure 4 and Table S1, all reactions in path B have higher barriers than A, C, and D, indicating that aromatic radicals retard defunctionalization of the side group. As shown in Table S4, the average Ru−C distance in all species in path B is shorter than those in paths A and C, underscoring stronger interactions of the unsaturated aryl group with Ru, which prohibits local geometries' adjustments during the bond breaking and increases the strain in the transition states.

The activation barrier of dehydrogenation (C−H bond cleavage) decreases sequentially in paths D and B. In all paths, the dehydrogenation of R−CH_3 possesses a higher barrier than that of R−CH_2*. In paths A and C, C−H scission from R−OCH* requires a higher barrier than R−OCH_2*. All C−H scissions in A, B, and C have higher barriers than those in D, indicating that the aromatic groups retard the C−H scission. For RO−C bond scissions in all paths, the RO−CH_3 bond has the highest barriers, followed by RO−CH_2*, RO−CH*, and RO−CH*. Unlike the C−H bonds, the aromatic rings in paths A and C reduce the barriers for breaking the O−C bonds, and the reactions become more exothermic. For Ar−OR bond scissions, the barrier gradually decreases with increasing defunctionalization level. The reactions in path A have the lowest barriers, followed by path C and path B. For all bond-breaking types (Ar−O, ArO−C, and C−H), reactions in path B have much higher barriers than those in paths A and C (Figure 5d). Given the higher barriers of 5−5 bond scissions,

https://doi.org/10.1021/acssuschemeng.1c04838
ACS Sustainable Chem. Eng. 2021, 9, 16143−16152

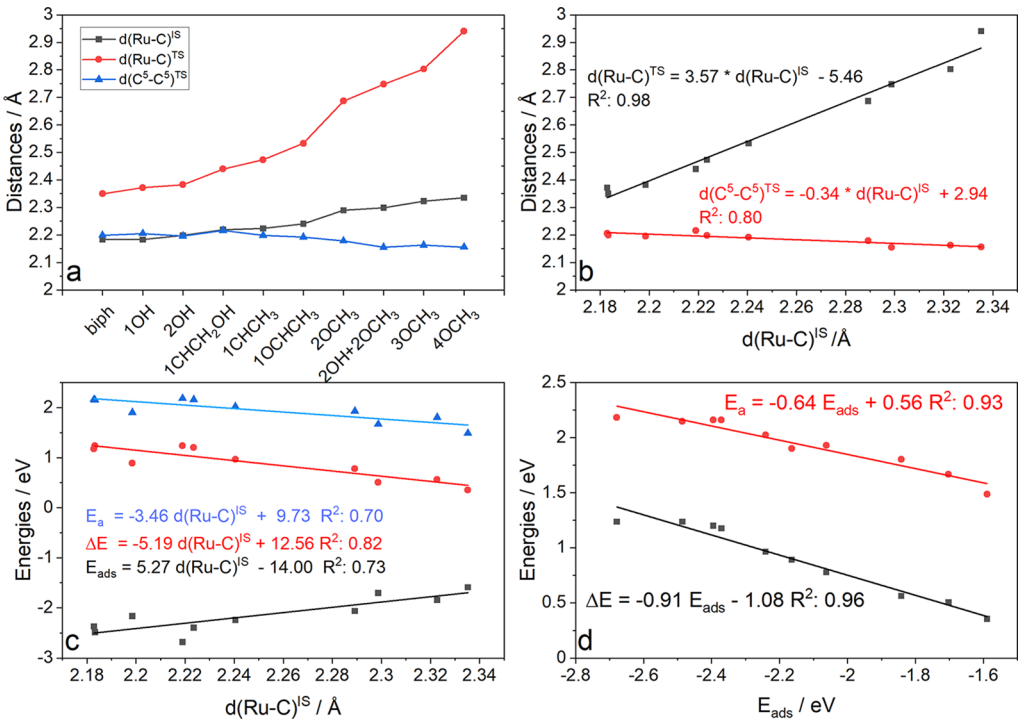

Figure 6. (a) Average Ru−C distances in initial structures (d(Ru−C)^{IS}) and transition states (d(Ru−C)^{TS}) and C−C bond lengths in TS (d(C^5−C^5)^{TS}) in different substituted Ar−H models. In the x-axis, the number indicates the ring location followed by the species replacing an H at this location. (b) Linear relationships between distances in TS (d(Ru−C)^{TS}, d(C^5−C^5)^{TS}) and IS (d(Ru−C)^{IS}). (c) Linear relationship between energies properties (E_{ads}, E_a, and ΔE) and d(Ru−C)^{IS}. (d) Linear variations of E_a and ΔE_a with reducing adsorption strength.

the decompositions from the functional groups are more likely to proceed from the dimer structures. This agrees qualitatively with the experimental study by Wang et al., showing the fully decomposed functional group in the one-pot lignin catalytic conversion over the Ru/$NbOPO_4$ catalyst.[3] The partial pressure of hydrogen should also play a role, as the first two dehydrogenations in Ar−OCH_3 are nearly thermoneutral and reversible. Once the C−O in the Ar−OC bond breaks, the chemistry becomes irreversible. The C−C cracking from A2 at modest pressures of hydrogen appears as the preferred pathway to monoaromatics but is not competitive with the dehydrogenation, demethylation, and hydrodeoxygenation.

Substitution Effects and BEP Relationships. As depicted in Figure 1, different functional groups (mainly −OCH_3) can exist at various locations of the aromatic rings. Substitution effects on adsorption and 5−5 bond scission were studied by adding relevant functional groups to the structures in Figure 3. For simplicity, the biphenyl is labeled as Ar−H. The substituted geometries and their adsorption energies, reaction energies, and barriers of the 5−5 bond scissions are listed in Tables S5 and S6. The adsorption energies are mainly determined by the interactions of the aromatic ring with the Ru atoms. Thus, the binding strength of molecules is intrinsically reflected in the Ru−C distance. As shown in Figure 6a, the Ru−C distances in both the initial state (d(Ru−C)^{IS}) and transition state (d(Ru−C)^{TS}) increase with more functional group substitutions and d(Ru−C)^{TS} is more sensitive to substitutions. More interestingly, with increasing d_{C-Ru}, the Ar−Ar bond length (d(C^5−C^5)^{TS}) in the TS is gradually shortened, implying that the transition states of species containing functional groups occur earlier. Figure 6b demonstrates the positive linear relationship between d(Ru−C)^{TS} and d(Ru−C)^{IS} and the negative relationship between d(C^5−C^5)^{TS} and d(Ru−C)^{IS}. This again implies that the substitutions increase the Ru−C distances of both the initial and transition states and promote the 5−5 bond breaking. In Figure 6c, the linear relationship between the adsorption energies (E_{ads}) and the d(Ru−C)^{IS} indicates that the structures with the shorter d(Ru−C) bind more strongly to the Ru surface, as expected, based on bond conservation arguments. The corresponding reaction barrier and energies are reduced, demonstrating that the functional groups weaken the species' adsorption and lower the 5−5 bond scission barrier (E_a). The linear relationship in Figure 6c can predict the reaction barrier rapidly using geometric properties. However, the d(Ru−C) values are not straightforward to obtain because DFT calculations must be conducted to determine the geometries and distances (an accurate force field could also be used). As d(Ru−C) is a descriptor for the adsorption energy, the scaling between d(Ru−C) and E_a can be transformed into one for E_{ads} and E_a (Figure 6d). E_{ads} can be obtained via an estimation method, such as group additivity, at a low computational cost.[44−46] Thus, the relation between E_{ads} and E_a is promising for barrier predictions. Also, we discover a BEP between E_{ads} and ΔE (R^2 of 0.90). As E_a and ΔE are linearly related to E_{ads}, a BEP relationship between ΔE and E_a for large molecules can be established.

5−5 bond scission can occur in eight intermediates in the reaction network (Figure 4), and a good BEP relationship holds (Figure 5). Since most intermediates (from A1 to A6) are hydrogen-deficient, they bind stronger than stable molecules (A0 and A7) and may be affected differently by substitutions. For this reason, we further investigated the substitution effect of −OCH_3 groups on the 5−5 scission of A4 (Ar−O*), A6 (Ar*), and A7 (ArH) species. There are 36, 36, and 32 species in A4-, A6-, and A7-derived intermediates

https://doi.org/10.1021/acssuschemeng.1c04838
ACS Sustainable Chem. Eng. 2021, 9, 16143−16152

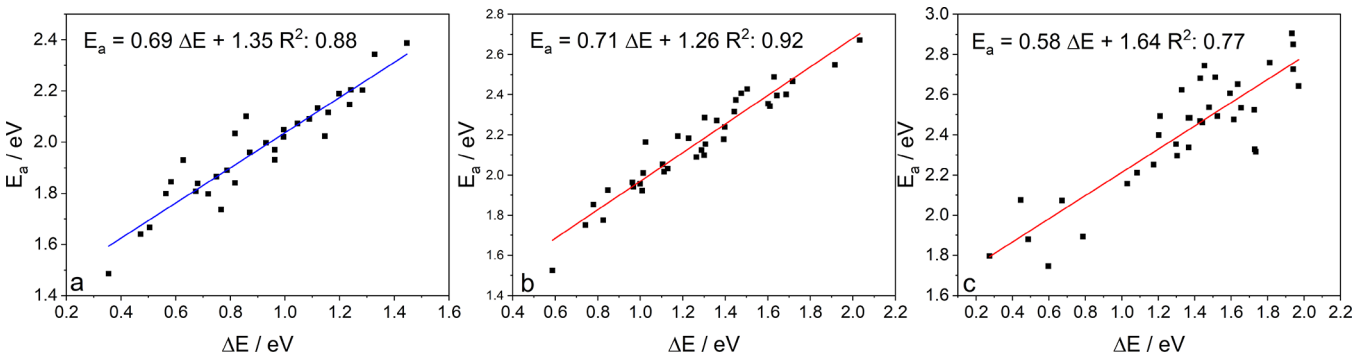

Figure 7. BEP relationships for 5−5 bond scission from (a) ArH (A7), (b) ArO* (A4), and (c) Ar* (A6) substituted species.

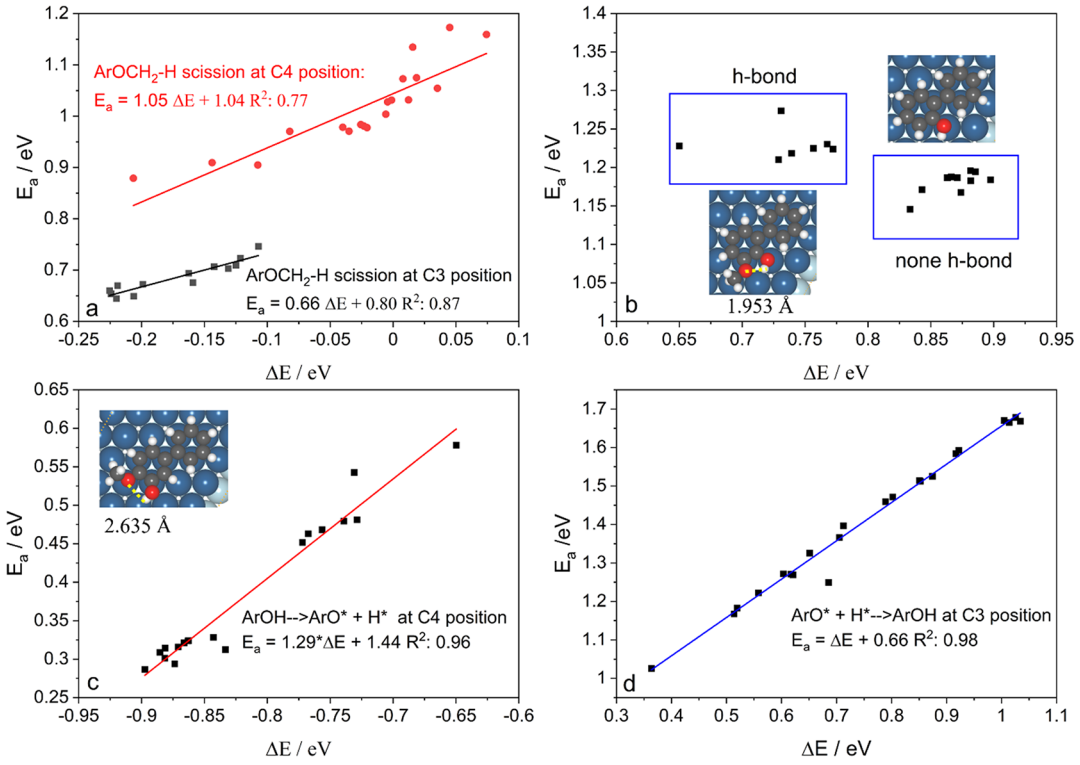

Figure 8. (a) BEP relationships for C−H bond scission and (b) hydrogen bond effects on ArO−H bond formation at the C4 position. (c) BEP relationship for ArO−H bond dissociation at the C4 position and (d) BEP relationship for the ArO−H bond formation at the C3 position.

(Table S4), respectively, containing a different number of −OH and $-OCH_3$ groups. For Ar−O* species, the highest, lowest, and average activation barriers for 5−5 scission are 2.67, 1.52, and 2.16 eV, respectively. These are larger than the barriers in the Ar−H substituted species (2.38, 1.48, and 1.97 eV), underscoring that the 5−5 bond is more challenging to break from the surface radical species. For Ar* species, the highest, lowest, and average activation barriers are 2.90, 1.75, and 2.41 eV, respectively, showing that the 5−5 bond cleavage becomes even more difficult. As shown in Figure 7a,b, good BEP relationships exist for ArH and ArO* species. However, this linear relationship deteriorates for the Ar* species (R^2 = 0.76). Specifically, deviations increase for species with largely distorted surface aromatic rings. For all substitutions in each group, the 5−5 bond cleavage barriers decrease with increasing number of $-OCH_3$ groups. As the content of $-OCH_3$ differs with the lignin source, containing various H, G, and S units (Figure 1), we conclude that 5−5 bonds from grass lignin (type H-G-S)[1] are easier to break, followed by softwood (type G-S) and then hardwood (type G). Since the binding energy decreases with increasing number of functional groups in the reactant (Table S7), site-blocking species (C* and O*) from $-OCH_3$ decomposition are favored and this lowers the catalytic activity. Therefore, controlling the H_2 pressure is crucial to remove C* and O* for preventing catalyst deactivation.

Since the C−H, Ar−OCH_3, ArO−H, and Ar−OH scissions are essential, we examine substitution effects for all of these. Given the presence of $-OCH_3$ at C3 or C4, we further examine substitution effects at both locations. Substitution effects on ArO−C and ArOC−H breakings from Ar−OCH_2* or Ar−OCH* were ignored due to their low activation barriers. As shown in Figure 8a and Table S8, C−H scission barriers at C3 are about 0.20 eV lower than at C4 positions. The reaction energies vary by about 0.15 and 0.30 eV at locations 3 and 4, implying that reactions at the latter are more sensitive to functional groups. BEP relationships with R^2 values of 0.87 and 0.77 are established.

https://doi.org/10.1021/acssuschemeng.1c04838
ACS Sustainable Chem. Eng. 2021, 9, 16143−16152

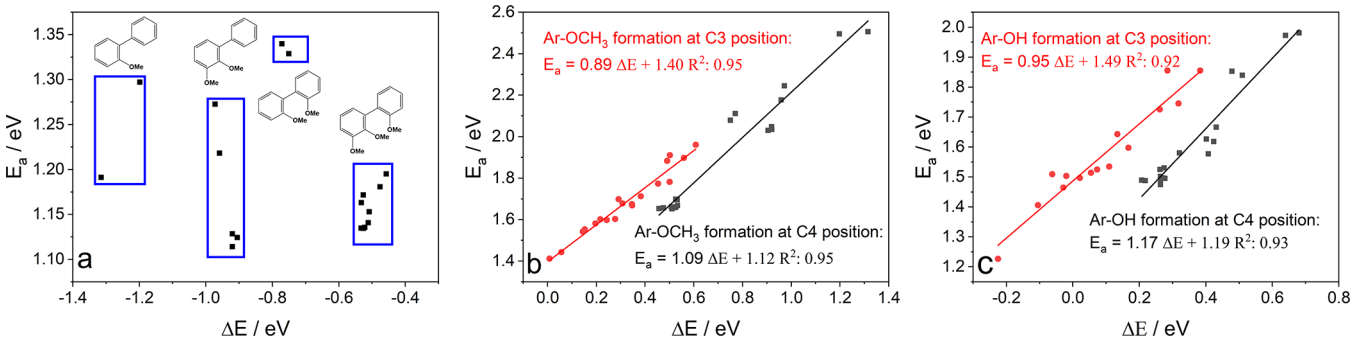

Figure 9. (a) Steric effects on Ar−OCH_3 bond scission. BEP relationships for (b) Ar−OCH_3 and (c) Ar−OH bond formations.

Figure 8b correlates the reaction energies and barriers for O−H bond formation of the C4 location. The barriers vary by as much as 0.13 eV. Data is classified into hydrogen-bond (H-bond) and no-H-bond regions, with average reaction barriers/energies of 1.23/0.73 and 1.18/0.87 eV, respectively. Due to the H-bond formation, the reaction becomes less endothermic by 0.13 eV and slightly kinetically unfavorable by 0.05 eV. The energy variations are 0.06 eV (H-bond) and 0.05 eV (no-H-bond), respectively, showing that the O−H bond formation is hardly affected by the substitutions. The slight energy variation of the barrier implies a poor BEP relationship. Instead, a BEP relationship for the reverse reaction (the O−H scission) is established with an R^2 of 0.96 (Figure 8c). For location C3, the −OH is above the fcc site and the H-bond between the −OH and the adjacent −OCH_3 group in the products is weaker than that in G4 because its bond length is much longer than in G4 (2.635 Å *vs* 1.953 Å). The BEP relationship for the O−H bond formation has an R^2 of 0.98 (Figure 8d). The reaction barriers and energies vary by as much as 0.65 and 0.67 eV, respectively. The average reaction barriers/energies at the C3 and C4 locations are 1.42/0.76 and 1.20/0.82 eV, respectively. Compared to the C4 location, the wider variation is due to the significant structural changes where the hydrogenated O atom moves from an fcc site to a top site, and the aromatic rings move from fcc sites to hcp sites. As the transition structures are similar to the products, the average reverse barrier of the O−H scission is nearly constant at 0.66 eV (within 0.05 eV from each other).

The average bond-breaking barriers in Ar−OCH_3 at C3 and C4 positions are 1.36 and 1.19 eV and vary by as much as 0.13 and 0.26 eV, respectively, showing that the Ar−OCH_3 bond breaking at the C4 location is kinetically favorable and more sensitive to the functional groups. As shown in Figure 9a, there are four subsets related to the four substituted cases. The Ar−OCH_3 bond breaking becomes thermodynamically more favorable with increasing steric effects. More structural details are listed in Table S10. The adjacent −OCH_3 substitution (structure 1 *vs* 7 and structure 6 *vs* 14 in Table S11) mainly affects the angles between the two bonds by ∼10°, and the reaction becomes more exothermic by 0.2−0.3 eV. The −OCH_3 in the other aromatic ring (structure 1 *vs* 6 and structure 7 *vs* 14) affects the angle and the dihedral angle and makes reactions more exothermic by 0.4 eV. For Ar−OH bond breakings, the average barrier at C3 (1.49 eV) is 0.23 eV higher than at C4 (1.26 eV). The barriers for various substitutions vary by 0.26 and 0.20 eV at C3 and C4 positions. Like the ArO−H cases in Figure 8c,d, good BEP relationships at the C3 and C4 positions are found for Ar−OCH_3 and Ar−OH bond formations, instead of scission (Figure 9b,c).

CONCLUSIONS

In an effort toward understanding lignin catalytic depolymerization chemistry and improving catalysts, we conducted many DFT calculations on van der Waals and substitution effects on adsorption, reaction energies, and the C−C bond scission barrier of the 5−5 linkage on Ru(0001) using 2-methoxy-1,1′-biphenyl as a starting model compound (probe molecule). The 5−5 linkage in lignin is the most commonly found and harder to break and controls the entire process, including monomer yields, processing conditions, and energy use. We propose a foundational reaction network to understand the rich chemistry and substitution effects systematically. The adsorption and bond scissions (5−5, O−H, C−H, and C−O) in various substituted biphenyl compounds in lignin were further studied via DFT. Yet, studying an entire biopolymer chain remains a challenge for future studies. The van der Waals interactions significantly increase the binding strength of model compounds by ∼0.90 eV per aromatic group but slightly affect reaction energies and barriers, consistent with a prior work on smaller molecules. We observed a linear relationship between the binding energy and the distance of aromatic C and surface Ru atoms. The adsorption of substituted 5−5 compounds becomes weaker and the 5−5 cleavage barrier decreases with increasing number of −OCH_3 in the aromatic ring. We predict that 5−5 bonds from grass lignin (type H-G-S) are easier to break than softwood (type G-S) and more so than hardwood (type G).

Interestingly, Ru exhibits modest C−C bond scission barriers in some of the intermediates of the network. Unfortunately, reactions in the side group −OCH_3 proceed faster than the 5−5 bond scission, leading first to complete defunctionalization in our model compound before C−C scission can occur. On the other hand, the 5−5 linkage scission from intermediates (Ar−H, Ar−O*, and Ar* substituted species) has a significant barrier, explaining its resistance to depolymerization. Based on the BEP relationship for 5−5 scission from various intermediates and decomposition product analysis, methods like inhibiting demethylation, promoting the benzyl and phenoxy hydrogenations, and controlling the reaction conditions according to the reactants would facilitate 5−5 bond breakings.

The substitution of −OCH_3 in three species (ArH, Ar−O*, and Ar) exposes a BEP relationship for the 5−5 C−C bond breaking. Other critical reactions, such as Ar−O(CH_3, H), ArO−H, and ArOCH_2−H bond breaking and formation, at C3 and C4 positions also yield good BEP relationships. Such correlations could be used to build quantitative microkinetic models to compare to relevant experimental data and improve

https://doi.org/10.1021/acssuschemeng.1c04838
ACS Sustainable Chem. Eng. 2021, 9, 16143−16152

our understanding of lignin chemistry. Finally, our work demonstrates that the C−H and C−O bond scissions in mono- and biaromatic groups differ from those in the methanol decomposition reaction, highlighting the importance of correctly choosing probe molecules for theoretical studies.

■ ASSOCIATED CONTENT

Supporting Information

The Supporting Information is available free of charge at https://pubs.acs.org/doi/10.1021/acssuschemeng.1c04838.

Adsorption energy of various species, reaction barriers, reaction energies, and illustrations of substituted structures (PDF)

■ AUTHOR INFORMATION

Corresponding Author

Dionisios G. Vlachos − *Catalysis Center for Energy Innovation, University of Delaware, Newark, Delaware 19716, United States; Department of Chemical and Biomolecular Engineering, University of Delaware, Newark, Delaware 19716, United States;* orcid.org/0000-0002-6795-8403; Email: vlachos@udel.edu

Author

Qiang Li − *Catalysis Center for Energy Innovation, University of Delaware, Newark, Delaware 19716, United States;* orcid.org/0000-0001-5568-2334

Complete contact information is available at: https://pubs.acs.org/10.1021/acssuschemeng.1c04838

Notes

The authors declare no competing financial interest.

■ ACKNOWLEDGMENTS

The work of Q.L. was supported by the Growing Convergence Research (GCR) program at the National Science Foundation (NSF) under award number NSF GCR CMMI 1934887. The Delaware Energy Institute gratefully acknowledges the support and partnership of the State of Delaware toward the RAPID projects.

■ REFERENCES

(1) Li, C.; Zhao, X.; Wang, A.; Huber, G. W.; Zhang, T. Catalytic transformation of lignin for the production of chemicals and fuels. *Chem. Rev.* **2015**, *115*, 11559−11624.

(2) Sun, Z.; Fridrich, B.; de Santi, A.; Elangovan, S.; Barta, K. Bright side of lignin depolymerization: toward new platform chemicals. *Chem. Rev.* **2018**, *118*, 614−678.

(3) Dong, L.; Lin, L.; Han, X.; Si, X.; Liu, X.; Guo, Y.; Lu, F.; Rudić, S.; Parker, S. F.; Yang, S.; Wang, Y. Breaking the Limit of Lignin Monomer Production via Cleavage of Interunit Carbon-carbon Linkages. *Chem* **2019**, *5*, 1521−1536.

(4) Fan, L.; Zhang, Y.; Liu, S.; Zhou, N.; Chen, P.; Cheng, Y.; Addy, M.; Lu, Q.; Omar, M. M.; Liu, Y.; Wang, Y.; Dai, L.; Anderson, E.; Peng, P.; Lei, H.; Ruan, R. Bio-oil from Fast Pyrolysis of Lignin: Effects of Process and Upgrading Parameters. *Bioresour. Technol.* **2017**, *241*, 1118−1126.

(5) Jing, Y.; Dong, L.; Guo, Y.; Liu, X.; Wang, Y. Chemicals from lignin: a review of catalytic conversion involving hydrogen. *ChemSusChem* **2020**, *13*, 4181−4198.

(6) Ha, J. M.; Hwang, K. R.; Kim, Y. M.; Jae, J.; Kim, K. H.; Lee, H. W.; Kim, J. Y.; Park, Y. K. Recent Progress in the Thermal and Catalytic Conversion of Lignin. *Renewable Sustainable Energy Rev.* **2019**, *111*, 422−441.

(7) Michel, C.; Gallezot, P. Why is Ruthenium An Efficient Catalyst for the Aqueous-phase Hydrogenation of Biosourced Carbonyl Compounds? *ACS Catal.* **2015**, *5*, 4130−4132.

(8) Verziu, M.; Tirsoaga, A.; Cojocaru, B.; Bucur, C.; Tudora, B.; Richel, A.; Aguedo, M.; Samikannu, A.; Mikkola, J. P. Hydrogenolysis of Lignin over Ru-based Catalysts: The Role of the Ruthenium in a Lignin Fragmentation Process. *Mol. Catal.* **2018**, *450*, 65−76.

(9) Li, H.; Song, G. Ru-catalyzed Hydrogenolysis of Lignin: Base-dependent Tunability of Monomeric Phenols and Mechanistic Study. *ACS Catal.* **2019**, *9*, 4054−4064.

(10) Van den Bosch, S.; Schutyser, W.; Vanholme, R.; Driessen, T.; Koelewijn, S. F.; Renders, T.; De Meester, B.; Huijgen, W. J. J.; Dehaen, W.; Courtin, C. M.; Lagrain, B.; Boerjan, W.; Sels, B. F. Reductive Lignocellulose Fractionation into Soluble Lignin-derived Phenolic Monomers and Dimers and Processable Carbohydrate Pulps. *Energy Environ. Sci.* **2015**, *8*, 1748−1763.

(11) Dong, L.; Xia, J.; Guo, Y.; Liu, X.; Wang, H.; Wang, Y. Mechanisms of $C_{aromatic}$-C Bonds Cleavage in Lignin over NbO_x-supported Ru Catalyst. *J. Catal.* **2021**, *394*, 94−103.

(12) Zhang, C.; Li, H.; Lu, J.; Zhang, X.; MacArthur, K. E.; Heggen, M.; Wang, F. Promoting Lignin Depolymerization and Restraining the Condensation via An Oxidation−hydrogenation Strategy. *ACS Catal.* **2017**, *7*, 3419−3429.

(13) Phongpreecha, T.; Liu, J.; Hodge, D. B.; Qi, Y. Adsorption of Lignin β-O-4 Dimers on Metal Surfaces in Vacuum and Solvated Environments. *ACS Sustainable Chem. Eng.* **2019**, *7*, 2667−2678.

(14) Lu, J.; Wang, M.; Zhang, X.; Heyden, A.; Wang, F. β-O-4 Bond Cleavage Mechanism for Lignin Model Compounds over Pd Catalysts Identified by Combination of First-principles Calculations and Experiments. *ACS Catal.* **2016**, *6*, 5589−5598.

(15) Ould Hamou, C. A.; Réocreux, R.; Sautet, P.; Michel, C.; Giorgi, J. B. Adsorption and Decomposition of a Lignin β-O-4 Linkage Model, 2-phenoxyethanol, on Pt (111): Combination of Experiments and First-Principles Calculations. *J. Phys. Chem. C* **2017**, *121*, 9889−9900.

(16) Li, Q.; López, N. Chirality, Rigidity, and Conjugation: A First-principles Study of the Key Molecular Aspects of Lignin Depolymerization on Ni-based Catalysts. *ACS Catal.* **2018**, *8*, 4230−4240.

(17) Gu, G. H.; Mullen, C. A.; Boateng, A. A.; Vlachos, D. G. Mechanism of Dehydration of Phenols on Noble Metals via First-Principles Microkinetic Modeling. *ACS Catal.* **2016**, *6*, 3047−3055.

(18) Lee, K.; Gu, G. H.; Mullen, C. A.; Boateng, A. A.; Vlachos, D. G. Hydrodeoxygenation Mechanism on Pt(111): Insights from Density Functional Theory and Linear Free Energy Relations. *ChemSusChem* **2015**, *8*, 315−322.

(19) Garcia-Pintos, D.; Voss, J.; Jensen, A. D.; Studt, F. Hydrodeoxygenation of Phenol to Benzene and Cyclohexane on Rh(111) and Rh(211) Surfaces: Insights from Density Functional Theory. *J. Phys. Chem. C* **2016**, *120*, 18529−18537.

(20) Chiu, C. C.; Genest, A.; Borgna, A.; Rösch, N. Hydrodeoxygenation of Guaiacol over Ru(0001): A DFT Study. *ACS Catal.* **2014**, *4*, 4178−4188.

(21) Shao, Y.; Xia, Q.; Dong, L.; Liu, X.; Han, X.; Parker, S. F.; Cheng, Y.; Daemen, L. L.; Ramirez-Cuesta, A. J.; Yang, S.; Wang, Y. Selective Production of Arenes via Direct Lignin Upgrading over a Niobium-based Catalyst. *Nat. Commun.* **2017**, *8*, 16104.

(22) Wang, S.; Temel, B.; Shen, J.; Jones, G.; Grabow, L. C.; Studt, F.; Bligaard, T.; Abild-Pedersen, F.; Christensen, C. H.; Nørskov, J. K. Universal Brønsted-Evans-Polanyi Relations for C−C, C−O, C−N, N−O, N−N, and O−O Dissociation Reactions. *Catal. Lett.* **2011**, *141*, 370−373.

(23) Wang, S.; Petzold, V.; Tripkovic, V.; Kleis, J.; Howalt, J. G.; Skúlason, E.; Fernández, E. M.; Hvolbae, K. B.; Jones, G.; Toftelund, A.; et al. Universal Transition State Scaling Relations for (De)-hydrogenation over Transition Metals. *Phys. Chem. Chem. Phys.* **2011**, *13*, 20760−20765.

(24) Greeley, J. Theoretical Heterogeneous Catalysis: Scaling Relationships and Computational Catalyst Design. *Annu. Rev. Chem. Biomol. Eng.* **2016**, *7*, 605−635.
(25) García-Muelas, R.; Li, Q.; López, N. Density functional theory comparison of methanol decomposition and reverse reactions on metal surfaces. *ACS Catal.* **2015**, *5*, 1027−1036.
(26) Ferrin, P.; Simonetti, D.; Kandoi, S.; Kunkes, E.; Dumesic, J. A.; Nørskov, J. K.; Mavrikakis, M. Modeling Ethanol Decomposition on Transition Metals: A Combined Application of Scaling and Brønsted−Evans−Polanyi Relations. *J. Am. Chem. Soc.* **2009**, *131*, 5809−5815.
(27) Li, Q.; García-Muelas, R.; López, N. Microkinetics of Alcohol Reforming for H_2 Production from a FAIR Density Functional Theory Database. *Nat. Commun.* **2018**, *9*, 526−528.
(28) Wang, S.; Vorotnikov, V.; Sutton, J. E.; Vlachos, D. G. Brønsted−Evans−Polanyi and Transition State Scaling Relations of Furan Derivatives on Pd (111) and Their Relation to Those of Small Molecules. *ACS Catal.* **2014**, *4*, 604−612.
(29) Abild-Pedersen, F.; Greeley, J.; Studt, F.; Rossmeisl, J.; Munter, T.; Moses, P.; Skulason, E.; Bligaard, T.; Nørskov, J. Scaling Properties of Adsorption Energies for Hydrogen-Containing Molecules on Transition-Metal Surfaces. *Phys. Rev. Lett.* **2007**, *99*, No. 016105.
(30) Gao, W.; Chen, Y.; Li, B.; Liu, S. P.; Liu, X.; Jiang, Q. Determining the Adsorption Energies of Small Molecules with the Intrinsic Properties of Adsorbates and Substrates. *Nat. Commun.* **2020**, *11*, 1196−1111.
(31) Calle-Vallejo, F.; Loffreda, D.; Koper, M. T. M.; Sautet, P. Introducing Structural Sensitivity into Adsorption−energy Scaling Relations by Means of Coordination Numbers. *Nat. Chem.* **2015**, *7*, 403−410.
(32) Kresse, G.; Hafner, J. *Ab-initio* Molecular-dynamics for Open-shell Transition-metals. *Phys. Rev. B* **1993**, *48*, 13115.
(33) Kresse, G.; Furthmüller, J. Efficient Iterative Schemes for *ab initio* Total-energy Calculations Using a Plane-wave Basis Set. *Phys. Rev. B* **1996**, *54*, 11169−11186.
(34) Kresse, G.; Furthmüller, J. Efficiency of *ab-initio* Total Energy Calculations for Metals and Semiconductors Using a Plane-wave Basis Set. *Comput. Mater. Sci.* **1996**, *6*, 15−50.
(35) Perdew, J. P.; Burke, K.; Ernzerhof, M. Generalized Gradient Approximation Made Simple. *Phys. Rev. Lett.* **1996**, *77*, 3865−3868.
(36) Blöchl, P. E. Projector Augmented-wave Method. *Phys. Rev. B* **1994**, *50*, 17953−17979.
(37) Kresse, G.; Joubert, D. From Ultrasoft Pseudopotentials to the Projector Augmented-wave Method. *Phys. Rev. B* **1999**, *59*, 1758−1775.
(38) Grimme, S.; Antony, J.; Ehrlich, S.; Krieg, H. A Consistent and Accurate *ab initio* Parametrization of Density Functional Dispersion Correction (DFT-D) for the 94 Elements H-Pu. *J. Chem. Phys.* **2010**, *132*, 154104.
(39) Lide, D., *CRC Handbook of Chemistry and Physics*; 84th ed.; CRC Press LLC: Boca Raton, FL (2003−2004).
(40) Henkelman, G.; Jónsson, H. Improved Tangent Estimate in the Nudged Elastic Band Method for Finding Minimum Energy Paths and Saddle Points. *J. Chem. Phys.* **2000**, *113*, 9978−9985.
(41) Henkelman, G.; Uberuaga, B. P.; Jónsson, H. A Climbing Image Nudged Elastic Band Method for Finding Saddle Points and Minimum Energy Paths. *J. Chem. Phys.* **2000**, *113*, 9901−9904.
(42) Held, G.; Braun, W.; Steinruck, H.-P.; Yamagishi, S.; Jenkins, S. J.; King, D. A. Light-Atom Location in Adsorbed Benzene by Experiment and Theory. *Phys. Rev. Lett.* **2001**, *87*, 216102.
(43) Braun, W.; Held, G.; Steinruck, H. P.; Stellwag, C.; Menzel, D. Coverage-dependent Changes in the Adsorption Geometries of Ordered Benzene Layers on Ru(0 0 0 1). *Surf. Sci.* **2001**, *475*, 18−36.
(44) Gu, G. H.; Vlachos, D. G. Group Additivity for Thermochemical Property Estimation of Lignin Monomers on Pt(111). *J. Phys. Chem. C* **2016**, *120*, 19234−19241.
(45) Vorotnikov, V.; Vlachos, D. G. Group Additivity and Modified Linear Scaling Relations for Estimating Surface Thermochemistry on Transition Metal Surfaces: Application to Furanics. *J. Phys. Chem. C* **2015**, *119*, 10417−10426.
(46) Vorotnikov, V.; Wang, S.; Vlachos, D. G. Group Additivity for Estimating Thermochemical Properties of Furanic Compounds on Pd(111). *Ind. Eng. Chem. Res.* **2014**, *53*, 11929−11938.

https://doi.org/10.1021/acssuschemeng.1c04838
ACS Sustainable Chem. Eng. 2021, 9, 16143−16152